Supporting Information

A solid composite electrolyte based on three-dimensional structured zeolite networks for high-performance solid-state lithium metal batteries

Zhaodi Luo,[a] Yuxin Cui,[ab] Zixuan Zhang,[a] Malin Li *[a] and Jihong Yu *[ab]

[a] *State Key Laboratory of Inorganic Synthesis and Preparative Chemistry, College of Chemistry, Jilin University, Changchun 130012, P. R. China.*

[b] *International Center of Future Science, Jilin University, Changchun 130012, P. R. China.*

** Corresponding authors. Emails: jihong@jlu.edu.cn (J. Y.); malinl@jlu.edu.cn (M. L.).*

Experimental Section

Materials

LUDOX®AS-40 colloidal silica was purchased from Sigma-Aldrich. Sodium hydroxide (NaOH), lithium chloride (LiCl), lithium bis(trifluoromethanesulfonyl)imide (LiTFSI) and acetonitrile (ACN) were purchased from Innochem. Polyurethane (PU) sponge with a thickness of 3 mm and aluminium foil were obtained from local suppliers. Poly(ethylene oxide) (PEO, M_n = 600,000) was purchased from Macklin. All reagents were used as received without further purification.

Synthesis of 3D Zeo

Preparation of crystallization solution: 4.17 g LUDOX AS-40 silica sol was added to 47.5 g deionized water and stirred at 60 °C for 2 h to ensure uniform dispersion. Meanwhile, 22.22 g NaOH and 0.3 g aluminium foil were dissolved in 50 g deionized water under stirring. After the solution having been clarified and cooled to room temperature, it was added dropwise into the silica dispersion under stirring. The resulting mixture was stirred at room temperature for 12 h until a transparent crystallization solution was obtained.

Preparation of 3D Zeo: PU sponge (5 cm × 3 cm × 3 mm) was annealed at 750 °C for 4 h in nitrogen atmosphere with a heating rate of 5 °C min^{-1} to yield carbonized PU sponge. After a 5-min plasma treatment for each side and a 120-min rest, the carbonized PU sponge was then immersed in the crystallization solution and heated at 60 °C for 24 h. The resulting sample was washed by deionized water and dried at 75 °C. Subsequently, the ion exchange was carried out by immersing the as-obtained sample in 1 M LiCl aqueous solution under stirring (200 rpm) at 60 °C for 4 h, and this ion-exchange step was repeated three times to obtain 3D Zeo.

Synthesis of composite solid electrolytes (CSEs)

Fabrication of 3D Zeo/PEO CSE: PEO was vacuum-dried at 50 °C for 24 h, while LiTFSI and the 3D Zeo were dried at 120 °C under vacuum for 24 h. Then, 0.88 g PEO was dissolved in 20 mL ACN, and the mixture was stirred for 8 h. After adding LiTFSI to maintain an [EO]:[Li^+] molar ratio of 18:1, the solution was stirred at 45 °C for 12 h to form a homogeneous LiTFSI-PEO precursor solution. The dried 3D Zeo was infiltrated by the LiTFSI-PEO precursor solution and placed in a vacuum oven. This process was repeated for about 7 times to fully fill the void of 3D Zeo. The as-prepared sample was sandwiched between two polytetrafluoroethylene (PTFE) films and hot-pressed at 100 °C. After drying in vacuum at 60 °C for 24 h, the as-obtained membranes were cut into 17-mm discs.

Fabrication of Zeo/PEO CSE: 3D Zeo was ground into fine powder and ultrasonically dispersed in ACN. The powder was then mixed with the LiTFSI-PEO precursor solution (the preparation method was mentioned above) and stirred for 12 h. The resulting slurry was cast onto a PTFE substrate via the doctor blade method. After being dried at room temperature for 6 h, followed by further vacuum-drying at 60 °C for 24 h, the Zeo/PEO CSE membrane was obtained. It is worth noting that the weight ratio of the 3D Zeo-derived powder in Zeo/PEO CSE is equal to the weight ratio of 3D Zeo in 3D Zeo/PEO CSE.

Preparation of PEO-based solid polymer electrolyte (SPE): The LiTFSI-PEO precursor solution was poured into a 20-mm PTFE mold and left at room temperature for 6 h to evaporate the ACN solvent. The membrane was then dried at 60 °C for 24 h under vacuum to obtained the SPE.

Materials characterization

The X-ray diffraction (XRD) measurements were performed on Rigaku D/MAX-2550 (Rigaku, Japan) using Cu Kα radiation (λ = 0.154 nm). Morphological and structural analyses were conducted using a JEOL JSM-6510 (JEOL, Japan) scanning electron microscope (SEM) equipped with energy dispersive spectroscopy (EDS). All the solid-state nuclear magnetic resonance (NMR) experiments were carried out on a Bruker Avance Neo 600 spectrometer (Bruker, USA). Fourier-transform infrared spectroscopy (FTIR) data was collected on a VERTEX 80v spectrometer (Bruker, Germany) with a wavenumber rang of 4000–500 cm^{-1} and a resolution of 4.0 cm^{-1} in an attenuated total reflection (ATR) mode. Raman spectra were characterized by a HS325 Raman microscope (Horiba, Japan) with a 325-nm wavelength laser. Thermogravimetric analysis (TGA) was performed using a NETZSCH STA 449 F3 thermal analyzer (NETZSCH, Germany) from room temperature to 800 °C at a heating rate of 10 °C min^{-1} under N_2 atmosphere. Differential scanning calorimetry (DSC) was conducted on a TA Instruments Q2000 system (TA Instruments, USA) under nitrogen flow at a heating rate of 10 °C min^{-1} using sealed aluminum pans. X-ray photoelectron spectroscopy (XPS) was used to explore the chemical states of the samples on Thermo Escalab 250 spectrometer (Thermo Fisher Scientific, USA). The time-of-flight secondary ion mass spectrometry (TOF-SIMS) was tested by FIB-SEM-Raman-TOF-SIMS All in One System (TESCAN C-TOF, Czech Republic) at a current of 0.5 nA and 30 kV. The analysis area is 100 × 100 μm at the cycled Li metal surface (plating/ stripping 50 cycles at 0.05 mA cm^{-2}).

Battery assembly

The electrochemical performance of the electrolytes was measured by assembling and testing the symmetric and full cells. The battery assembly was carried out in an Ar-filled glovebox with the oxygen and moisture content below 0.01 ppm, and the batteries were aged at 60 °C for 12 h before testing. For the symmetric cells, solid-state electrolytes (SSEs) membranes were sandwiched by two lithium foils or stainless steels (SS) and assembled into the CR2032 coin cell. For the full cells, $LiFePO_4$ (LFP) and $LiNi_{0.8}Co_{0.1}Mn_{0.1}O_2$ (NCM) were employed as the cathode materials. To improve the interfacial wettability of the batteries tested at room temperature, a controlled amount (~1.6 μL cm^{-2}) of 1 mol L^{-1} $LiPF_6$ in diethyl carbonate: ethylene carbonate with a volume ratio of 1:1 was added at the electrode–electrolyte interfaces. To prepared the cathode, active materials (80 wt%), Super P (10 wt%), and PVDF (10 wt%) as binder in NMP were mixed into a slurry and coated onto the carbon-coated Al foil. Subsequently, the electrodes were dried in a vacuum oven at 60 ℃ for 12 h, and then cut into disks with a diameter of 12 mm. The mass loading of $LiFePO_4$ on each disk is 1.2~1.5 mg cm^{-2}, and the mass loading of $LiNi_{0.8}Co_{0.1}Mn_{0.1}O_2$ cathode is 0.8~1.0 mg cm^{-2}. The thickness of Li foil is 450 μm.

Electrochemical Measurements

To analyze the ionic conductivities of the SSEs, SS were employed as the electrodes to assemble CR2032 coin cell, and the electrochemical impedance spectra (EIS) were recorded on a BioLogic VSP-300 electrochemical station in the frequency range of 7.0 MHz–0.1 Hz from room temperature (RT) to 60 °C. The ionic conductivity (σ) was calculated according to **Equation 1**:

$$\sigma = \frac{l}{R_\Omega S}$$

where σ is the ionic conductivity (S cm^{-1}), R_Ω is the impedance of electrolytes (Ω), l is the thickness of electrolyte membrane, and S is the contact area between electrolytes and SS electrode (cm^2).

The activation energy (E_a) of Li^+ transport was calculated based on **Equation 2**:

$$\sigma = \mathrm{A}e^{\frac{-E_a}{RT}}$$

where A is the pre-exponential factor, E_a is the activation energy of Li^+ transport (eV), R is the ideal gas constant (8.314 J mol^{-1} K^{-1}), and T is the absolute temperature (K).

The lithium ion transference numbers (t_{Li^+}) of the SSEs were tested with a Li|SSEs|Li symmetric cell via combining an EIS measurement and a direct current (DC) potentiostatic

polarization measurement. EIS was measured in a frequency range from 1.0 MHz to 0.1 Hz before and after the DC polarization. t_{Li^+} was calculated according to Modified Bruce-Vincent-Evans **Equation 3**:

$$t_{Li^+} = \frac{I_{ss}(\Delta V - I_0 R_0)}{I_0(\Delta V - I_{ss} R_{ss})}$$

where t_{Li^+} is the Li^+ transference number, ΔV is the polarization voltage amplitude (10 mV), I_0 and I_{ss} are the initial and steady-state currents, and R_0 and R_{ss} are the resistances before and after polarization, respectively.

The electrochemical stability window was evaluated by testing linear scanning voltammetry (LSV) curves of SS/electrolytes/Li cells at a scan rate of 1 mV s^{-1} from 2 to 6 V (*vs*. Li^+/Li).

The galvanostatic charge and discharge measurements were performed on LAND CT3004A battery testing systems to evaluate the cycling and rate performance of the symmetric and full cells. The LFP|SSEs|Li full cells were tested in a voltage range of 2.5–4.2 V at various C-rates (1.0C = 170 mA g^{-1}), and the NCM|SSEs|Li full cells were tested in a voltage range of 2.8–4.3 V at various C-rates (1.0C = 200 mA g^{-1}). EIS measurements were carried out in a frequency range from 7.0 MHz to 0.1 Hz on BioLogic VSP-300 electrochemical station.

Theoretical Calculations

The Vienna Ab Initio Package (VASP) was employed to perform all the density functional theory (DFT) calculations within the generalized gradient approximation (GGA) using the Perdew, Burke, and Enzerhof (PBE) formulation.[1-3] The projected augmented wave (PAW) potentials were applied to describe the ionic cores and take valence electrons into account using a plane wave basis set with a kinetic energy cutoff of 500 eV.[4,5] Partial occupancies of the Kohn–Sham orbitals were allowed using the Gaussian smearing method and a width of 0.05 eV. The electronic energy was considered self-consistent when the energy change was smaller than 10^{-5} eV. A geometry optimization was considered convergent when the force change was smaller than 0.05 eV/Å. Grimme's DFT-D3 methodology was used to describe the dispersion interactions.[6] The vacuum spacing perpendicular to the plane of the structure is 20 Å. The Brillouin zone integral utilized the surfaces structures of 2×2×1 monkhorst pack K-point sampling. Finally, the binding energies (E_b) were calculated according to **Equation 4**:

$$E_b = E_{ad/sub} - E_{ad} - E_{sub}$$

where $E_{ad/sub}$, E_{ad}, and E_{sub} are the total energies of the optimized adsorbate/substrate system, the adsorbate in the structure, and the clean substrate, respectively.

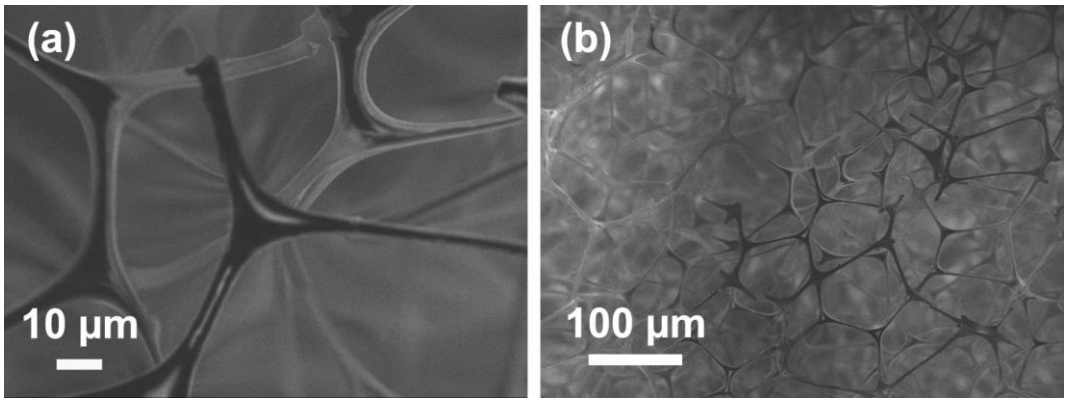

Fig. S1 SEM images of polyurethane (PU) sponge.

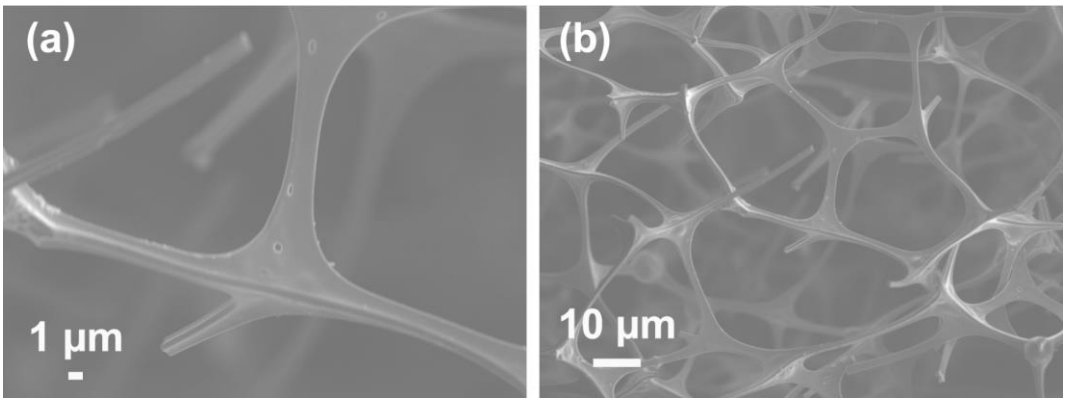

Fig. S2 SEM images of carbonized PU sponge.

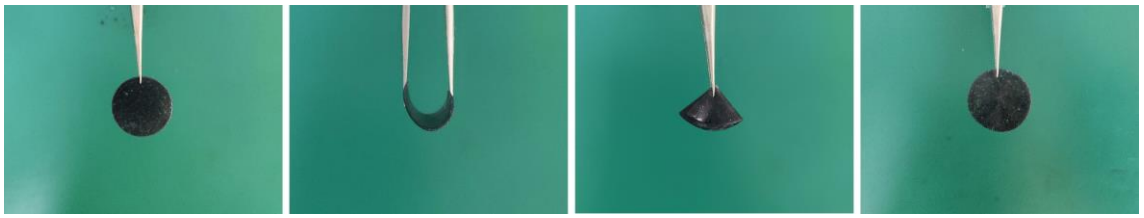

Fig. S3 Optical photographs of the 3D Zeo/PEO electrolyte.

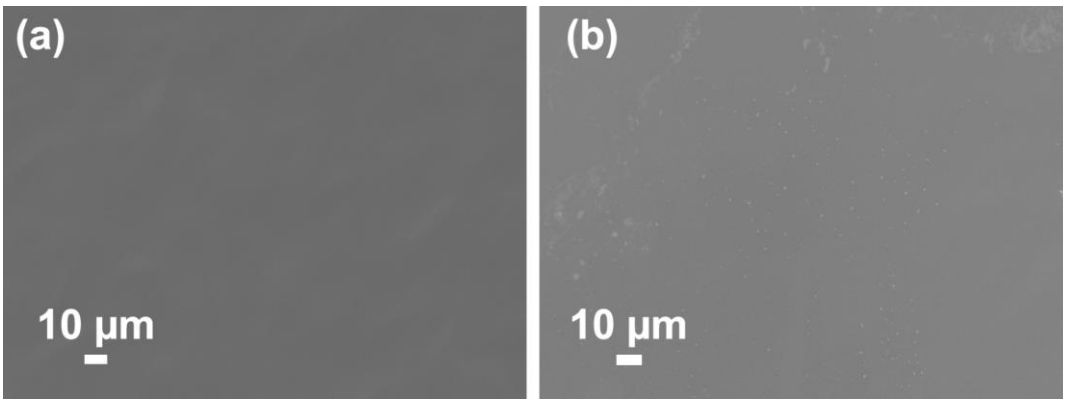

Fig. S4 SEM images of (a) SPE and (b) Zeo/PEO.

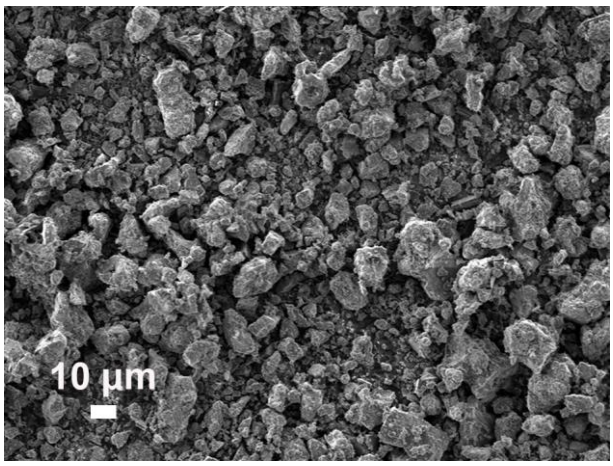

Fig. S5 SEM image of Zeo particles derived from 3D Zeo.

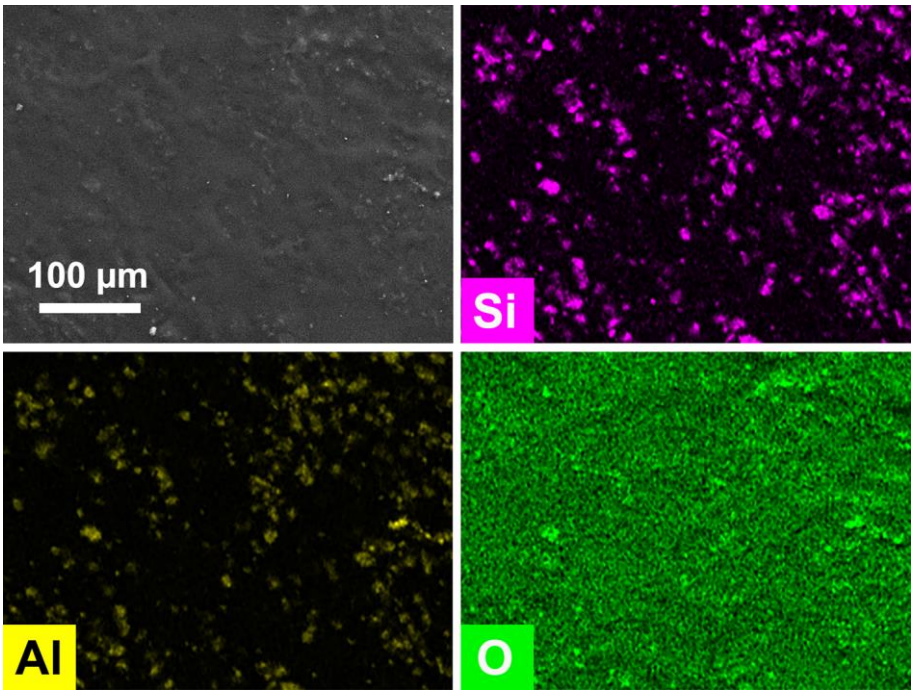

Fig. S6 EDS element mappings of Zeo/PEO.

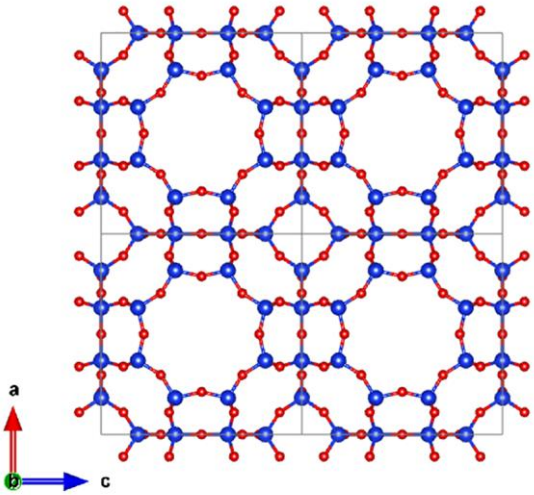

Fig. S7 Schematic illustration of the structure for **LTA**-type zeolite.

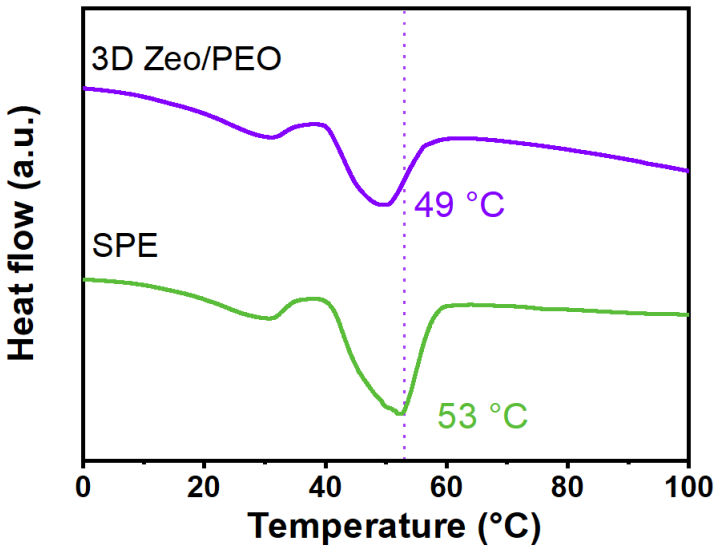

Fig. S8 DSC curves of SPE and 3D Zeo/PEO electrolytes.

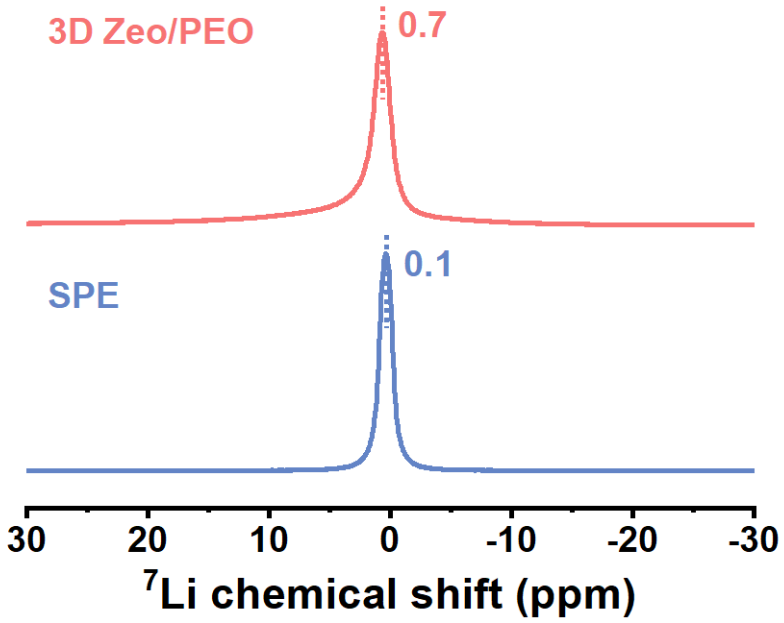

Fig. S9 ^{7}Li solid-state NMR spectra of SPE and 3D Zeolite/PEO.

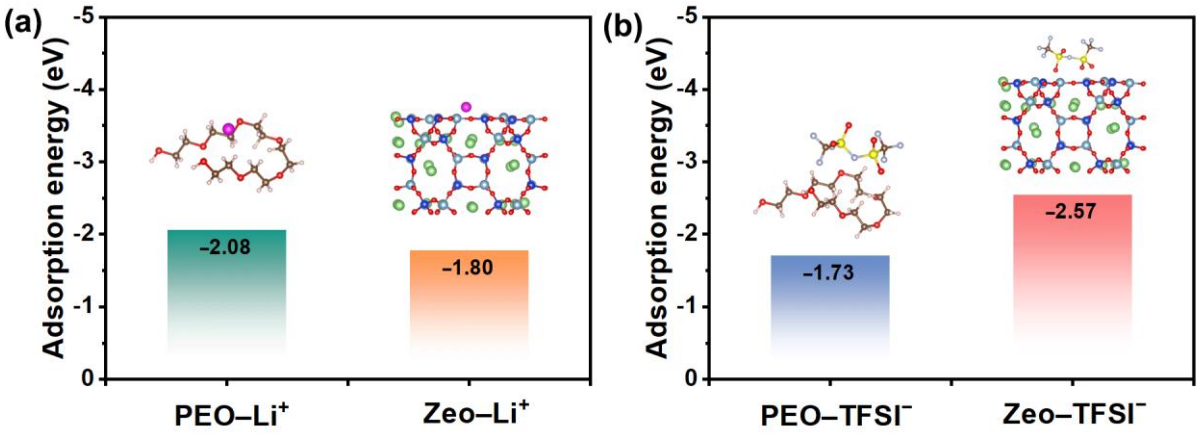

Fig. S10 Calculation of adsorption energies of (a) PEO–Li^+ and Zeo–Li^+, and (b) PEO–$TFSI^-$ and Zeo–$TFSI^-$.

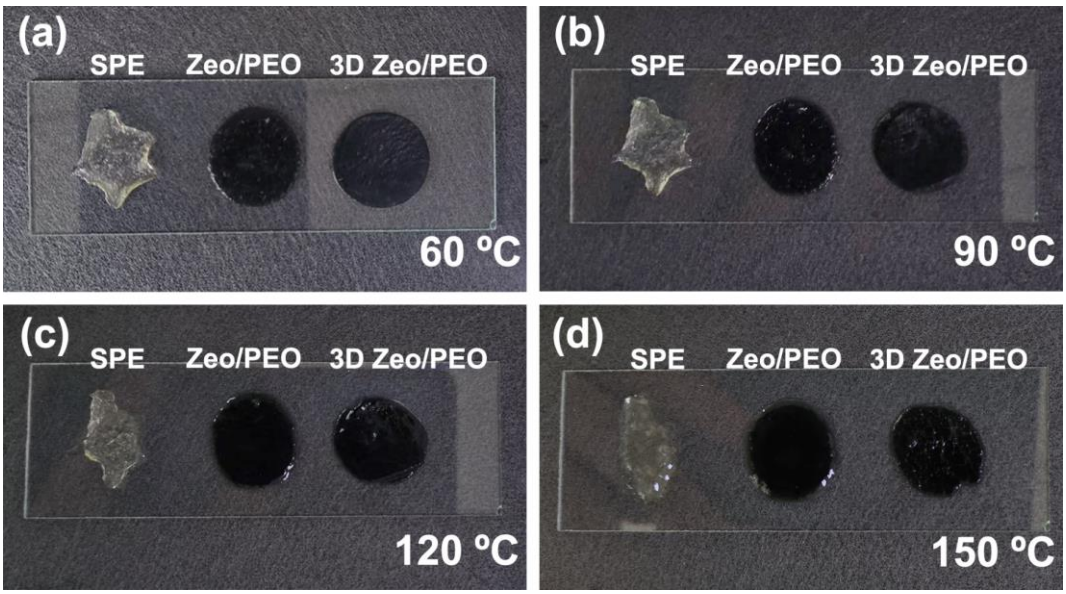

Fig. S11 Thermal stability of SPE, Zeo/PEO and 3D Zeo/PEO when placed at different temperatures for 0.5 h.

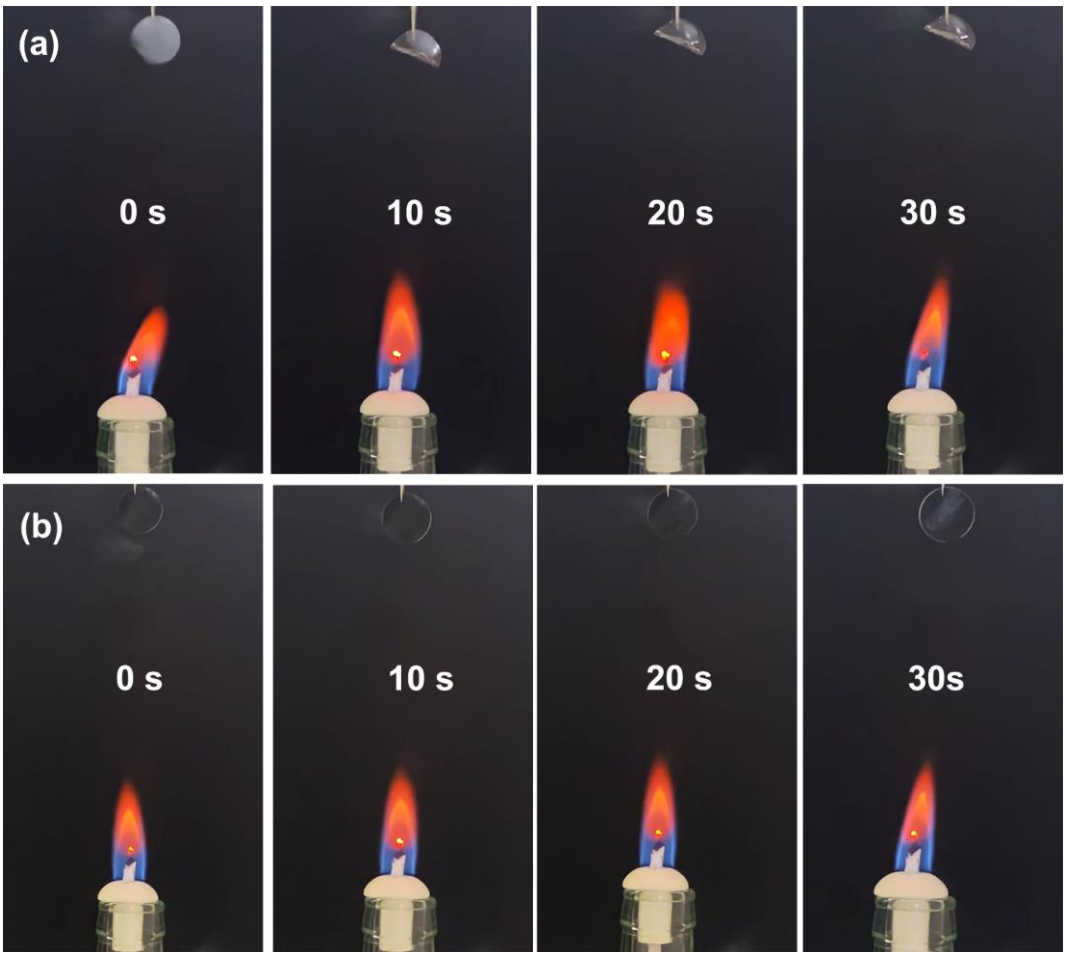

Fig. S12 Flame heating test for (a) SPE and (b) 3D Zeo/PEO electrolytes.

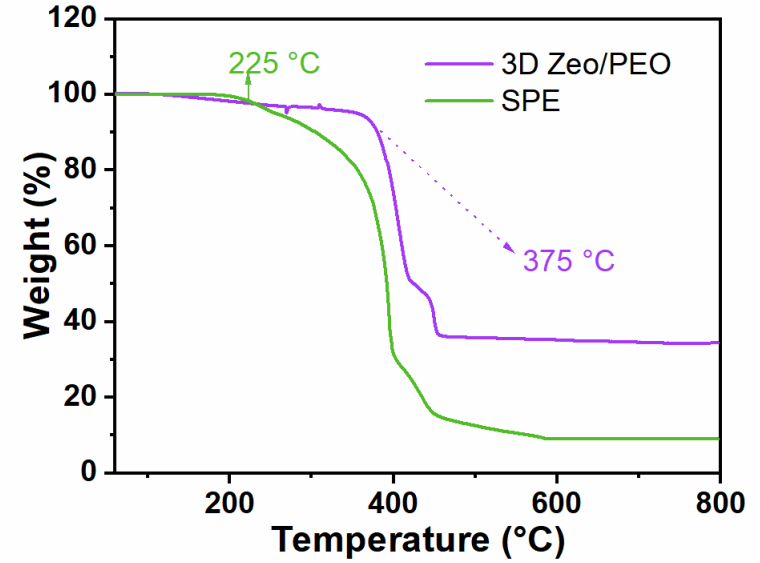

Fig. S13 TGA curves of SPE and 3D Zeo/PEO electrolytes.

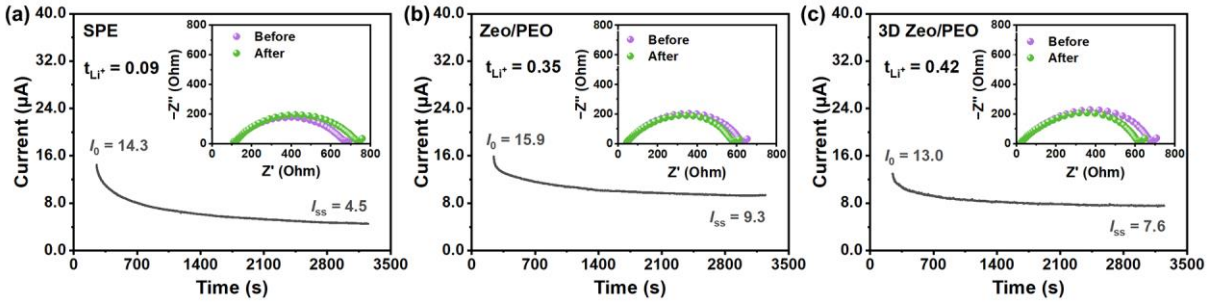

Fig. S14 Lithium ion transference numbers (t_{Li^+}) measurements of (a) PEO, (b) Zeo/PEO and (c) 3D Zeo/PEO at 60 °C.

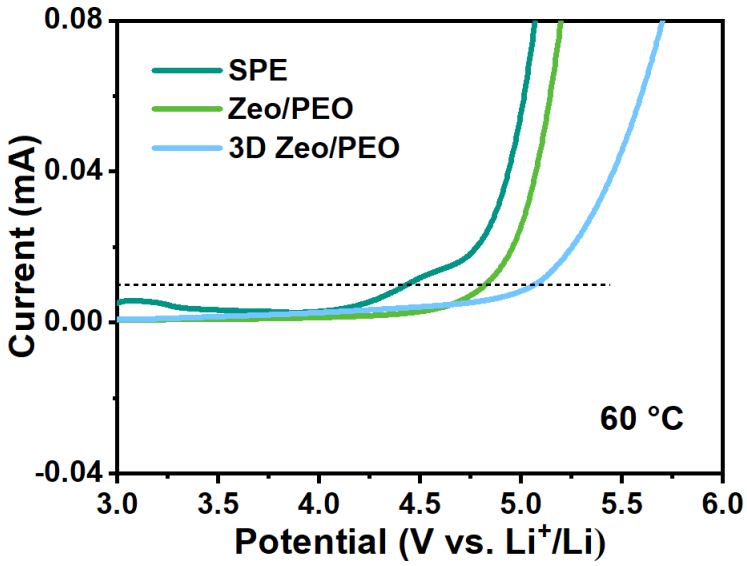

Fig. S15 LSV curves of PEO, Zeo/PEO and 3D Zeo/PEO electrolytes at 60 °C.

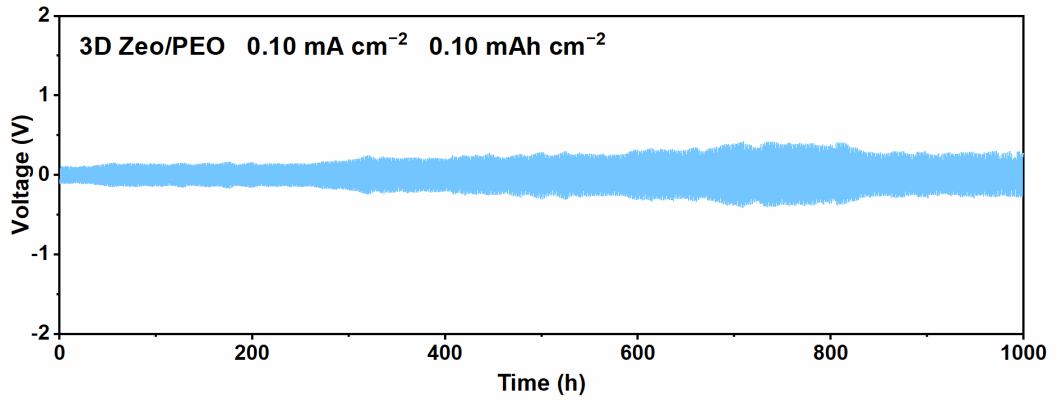

Fig. S16 Galvanostatic Li plating/stripping profiles of 3D Zeo/PEO symmetric cell at 0.10 mA cm^{-2} and 0.10 mAh cm^{-2}.

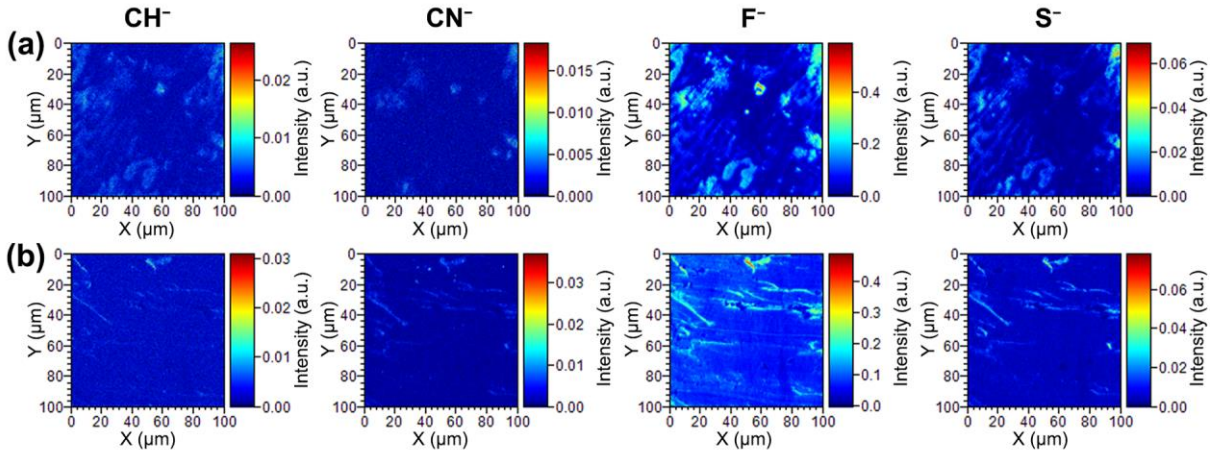

Fig. S17 Top-view 2D mappings of the TOF-SIMS sputtered volume on the SEI using (a) SPE and (b) 3D Zeo/PEO.

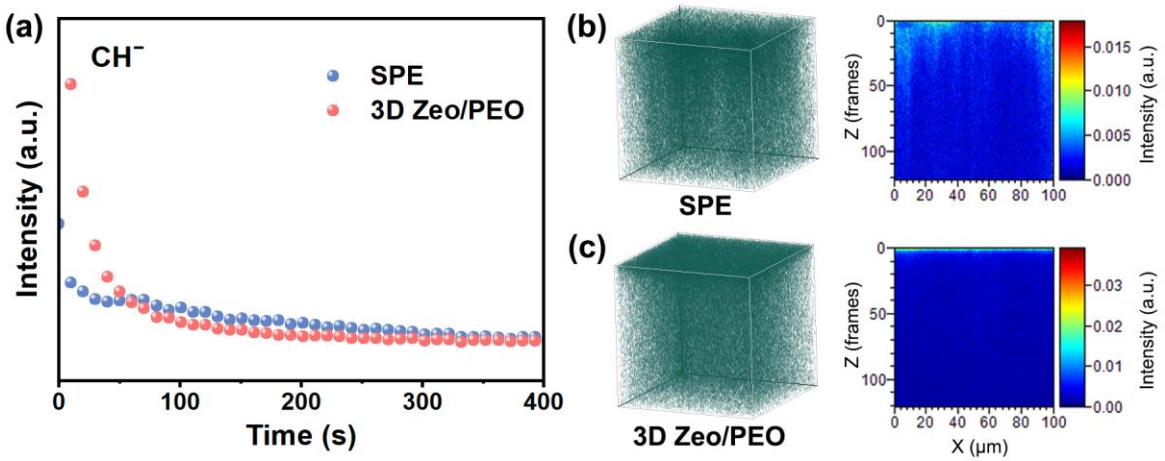

Fig. S18 (a) TOF-SIMS depth profiles for CH^-. 3D distribution mapping and corresponding cross-sectional 2D mappings of the sputtered volume on the SEI using (b) SPE and (c) 3D Zeo/PEO.

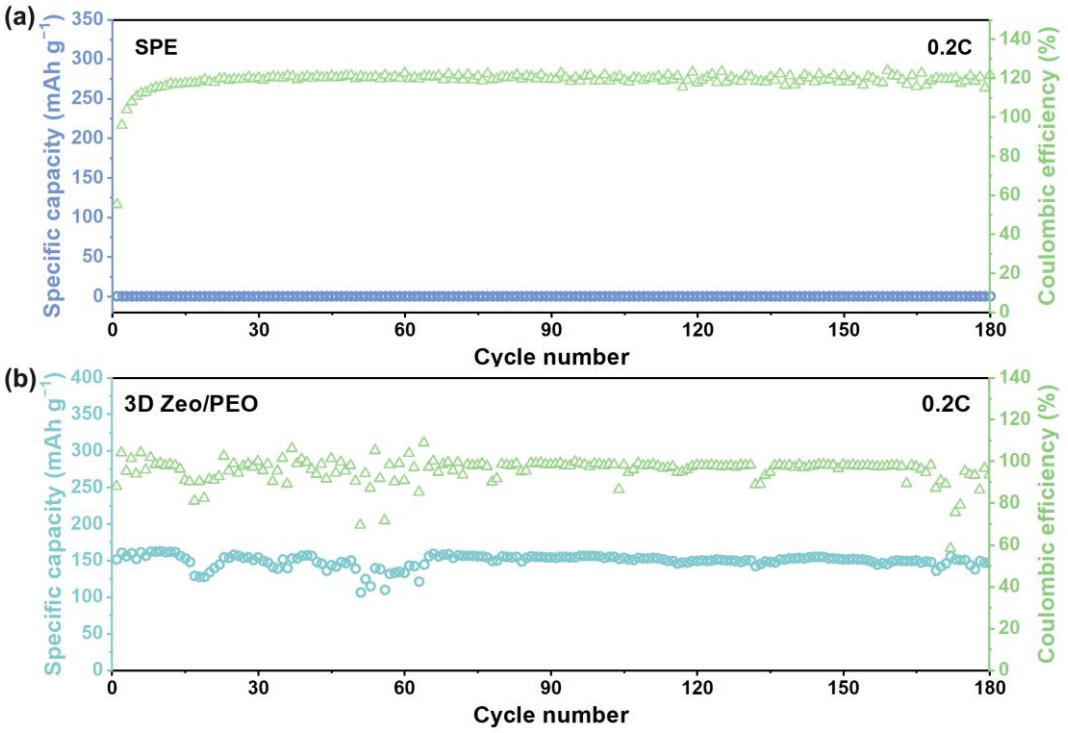

Fig. S19 Cycling performance of LFP|SSEs|Li full cells with (a) SPE and (b) 3D Zeo/PEO at 0.2 C and RT.

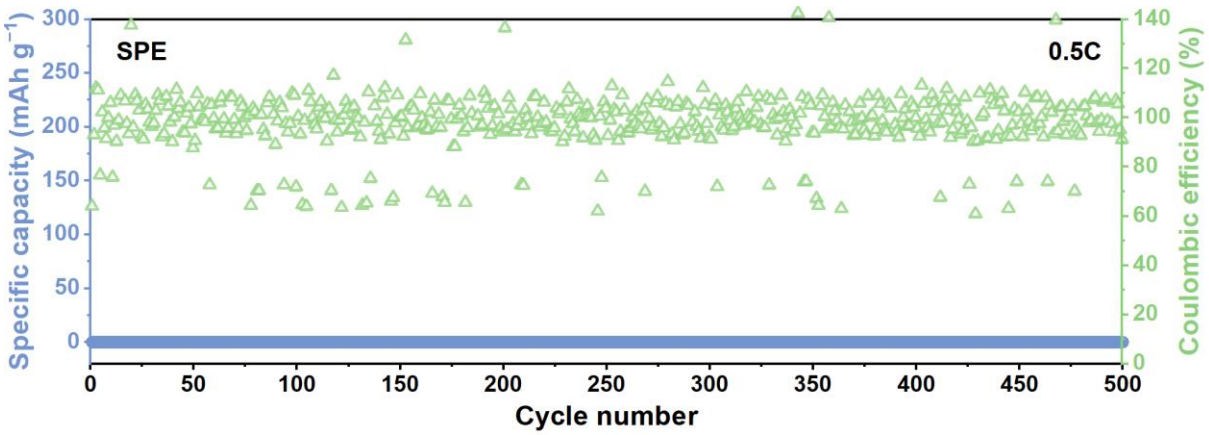

Fig. S20 Cycling performance of LFP|SPE|Li full cell at 0.5C and RT.

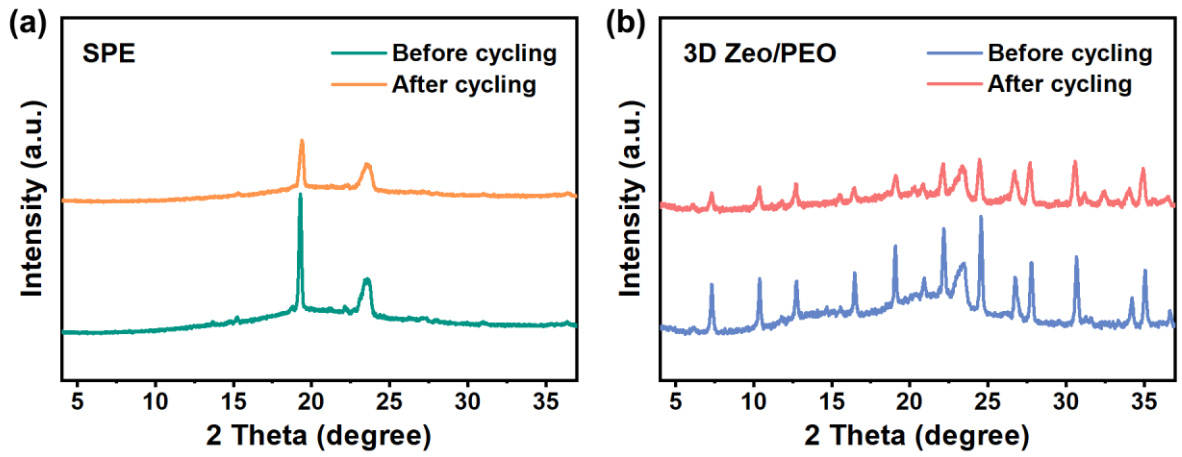

Fig. S21 XRD patterns of (a) SPE and (b) 3D Zeo/PEO before and after cycling at 60 °C. The XRD patterns of both cycled SPE and 3D Zeo/PEO electrolytes exhibit a slight reduction in peak intensity, especially the peak at 19.2°, indicating a loss of crystallinity after cycling. No new diffraction peak appears, demonstrating the absence of new crystalline phases.

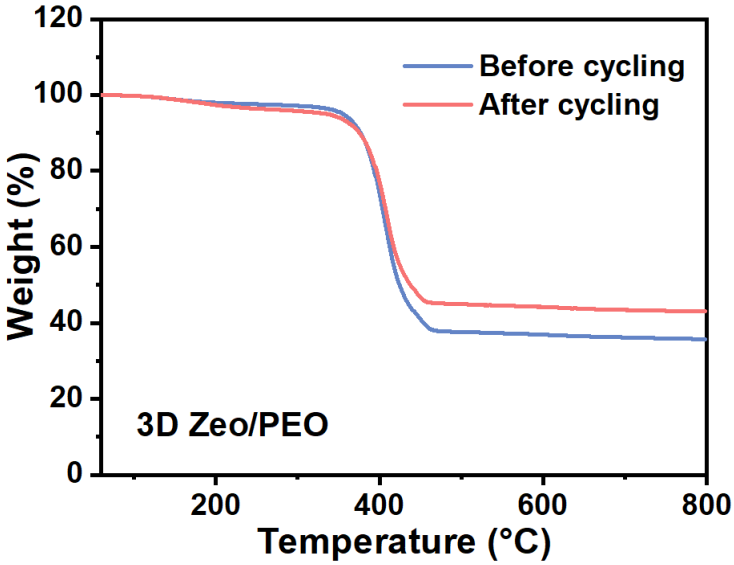

Fig. S22 Comparison of TGA curves of 3D Zeo/PEO before and after cycling at 60 °C. The onset decomposition temperature remains essentially unchanged after cycling, suggesting that there is no significant change in the bulk thermal stability of PEO component. However, it is worth noting that the stability of PEO at the interface between electrode and electrolyte can hardly be revealed by this test.

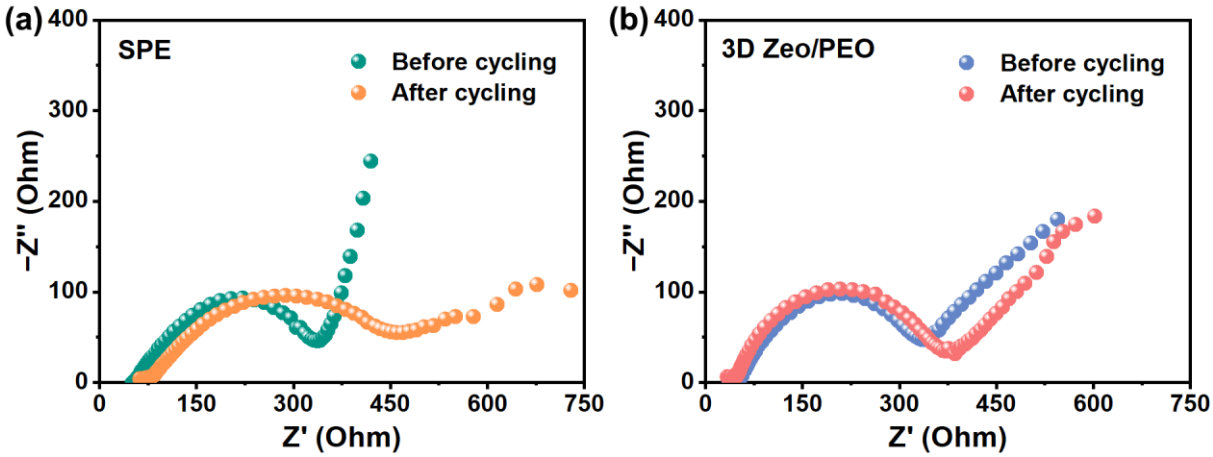

Fig. S23 Nyquist plots of LFP|SSEs|Li full cells with (a) SPE and (b) 3D Zeo/PEO before and after cycling at 60 °C. The charge transfer impedances (R_{ct}) of both SPE and 3D Zeo/PEO increase after cycling, indicating that the batteries undergo an interfacial degradation during cycling at 60 °C. This may be attributed to the compatibility of SSEs with cathode materials, and is probably the primary cause for the capacity fading of batteries cycled at 60 °C. In comparison with the battery using SPE, the battery using 3D Zeo/PEO exhibits a smaller increase in R_{ct} after cycling, consistent with the superior performance of 3D Zeo/PEO full cells at 60 °C.

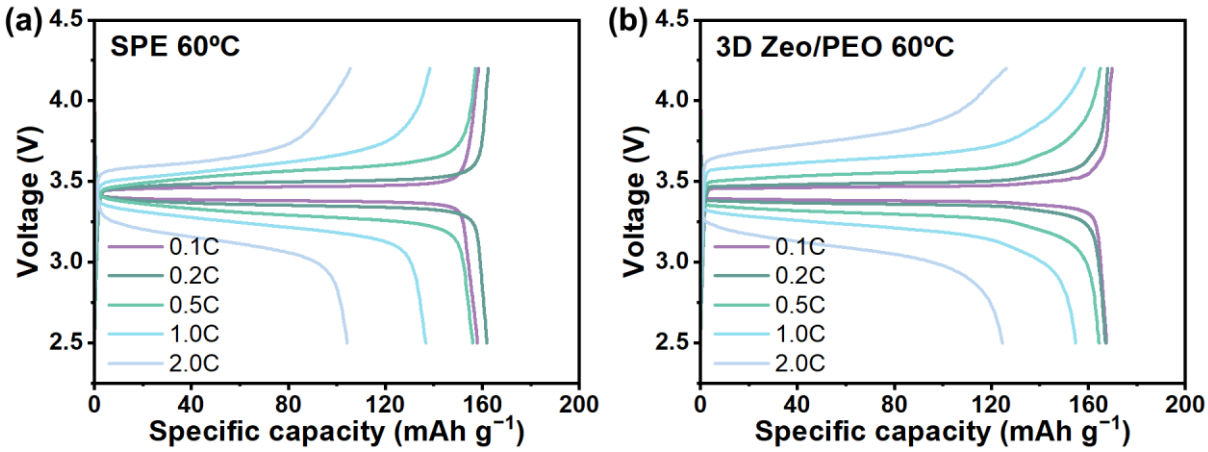

Fig. S24 Galvanostatic charge and discharge profiles of LFP|SSEs|Li full cells with (a) SPE and (b) 3D Zeo/PEO electrolytes at various current densities at 60 °C.

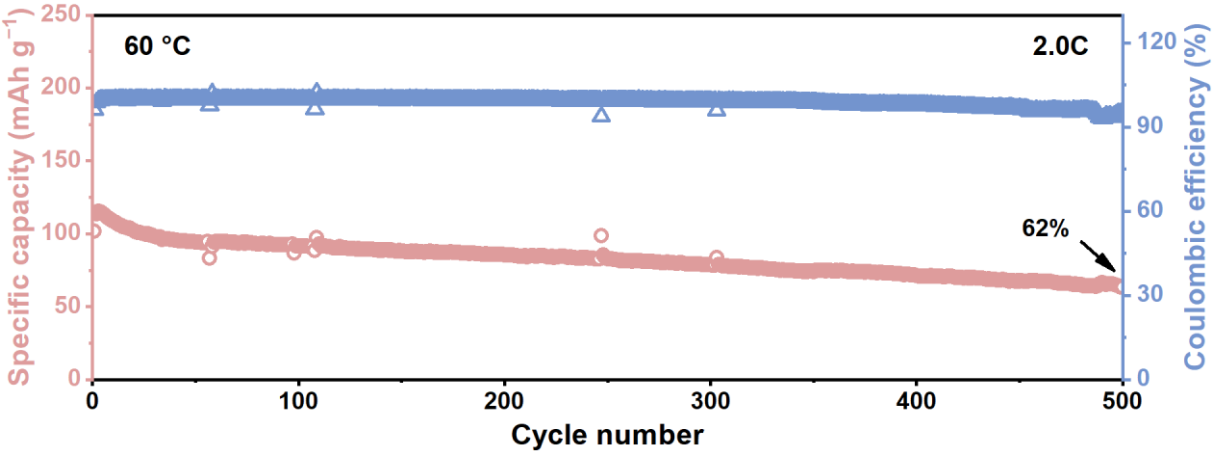

Fig. S25 Cycling performance of LFP|3D Zeo/PEO|Li full cell at 2.0C and 60 °C.

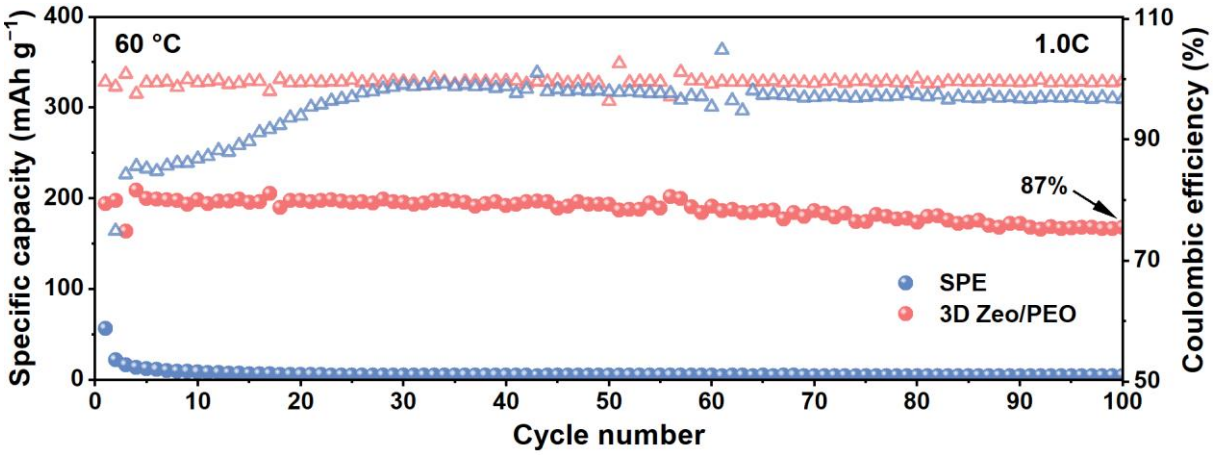

Fig. S26 Cycling performance of NCM|SSEs|Li full cells with SPE and 3D Zeo/PEO at 1.0C and 60 °C.

Table S1. Ionic conductivities (S cm^{-1}) of SPE, Zeo/PEO, and 3D Zeo/PEO measured at various temperatures.

Samples	RT	30 °C	40 °C	50 °C	60 °C
SPE	3.23×10^{-6}	4.89×10^{-6}	1.76×10^{-5}	1.26×10^{-4}	4.89×10^{-4}
Zeo/PEO	3.43×10^{-5}	5.63×10^{-5}	2.60×10^{-4}	3.84×10^{-4}	5.86×10^{-4}
3D Zeo/PEO	1.62×10^{-4}	2.06×10^{-4}	3.05×10^{-4}	4.92×10^{-4}	6.49×10^{-4}

References

1. G. Kresse, J. Furthmüller, Efficient iterative schemes for ab initio total-energy calculations using a plane-wave basis set, *Phys. Rev. B*, 1996, **54**, 11169–11186.
2. J. Perdew, P. K. Burke, M. Ernzerhof, Generalized gradient approximation made simple, *Phys. Rev. Lett.*, 1996, **77**, 3865–3868.
3. G. Kresse, D. Joubert, From ultrasoft pseudopotentials to the projector augmented-wave method, *Phys. Rev. B*, 1999, **59**, 1758–1775.
4. P. E. Blöchl, Projector augmented-wave method, *Phys. Rev. B*, 1994, **50**, 17953–17979.
5. S. Grimme, J. Antony, S. Ehrlich, H. Krieg, *J. Chem. Phys.*, 2010, **132**, 154104.
6. G. Henkelman, B. P. Uberuaga, H. Jonsson, *J. Chem. Phys.*, 2000, **113**, 9901.